

Changes in Sea Salt Emissions Enhance ENSO Variability

YANG YANG

Scripps Institution of Oceanography, University of California, San Diego, La Jolla, California, and Atmospheric Science and Global Change Division, Pacific Northwest National Laboratory, Richland, Washington

LYNN M. RUSSELL

Scripps Institution of Oceanography, University of California, San Diego, La Jolla, California

SIJIA LOU

Scripps Institution of Oceanography, University of California, San Diego, La Jolla, California, and Atmospheric Science and Global Change Division, Pacific Northwest National Laboratory, Richland, Washington

MARYAM A. LAMJIRI

Scripps Institution of Oceanography, University of California, San Diego, La Jolla, California

YING LIU, BALWINDER SINGH, AND STEVEN J. GHAN

Atmospheric Science and Global Change Division, Pacific Northwest National Laboratory, Richland, Washington

(Manuscript received 22 March 2016, in final form 8 August 2016)

ABSTRACT

Two 150-yr preindustrial simulations with and without interactive sea salt emissions from the Community Earth System Model (CESM) are performed to quantify the interactions between sea salt emissions and El Niño–Southern Oscillation (ENSO). Variations in sea salt emissions over the tropical Pacific Ocean are affected by changing wind speed associated with ENSO variability. ENSO-induced interannual variations in sea salt emissions result in decreasing (increasing) aerosol optical depth (AOD) by 0.03 over the equatorial central-eastern (western) Pacific Ocean during El Niño events compared to those during La Niña events. These changes in AOD further increase (decrease) radiative fluxes into the atmosphere by $+0.2$ (-0.4) W m^{-2} over the tropical eastern (western) Pacific. Thereby, sea surface temperature increases (decreases) by 0.2–0.4 K over the tropical eastern (western) Pacific Ocean during El Niño compared to La Niña events and enhances ENSO variability by 10%. The increase in ENSO amplitude is a result of systematic heating (cooling) during the warm (cold) phase of ENSO in the eastern Pacific. Interannual variations in sea salt emissions then produce the anomalous ascent (subsidence) over the equatorial eastern (western) Pacific between El Niño and La Niña events, which is a result of heating anomalies. Owing to variations in sea salt emissions, the convective precipitation is enhanced by 0.6–1.2 mm day^{-1} over the tropical central-eastern Pacific Ocean and weakened by 0.9–1.5 mm day^{-1} over the Maritime Continent during El Niño compared to La Niña events, enhancing the precipitation variability over the tropical Pacific.

1. Introduction

Aerosol particle emissions can substantially perturb Earth's radiative balance, and those emissions are affected by feedbacks from changing the Earth system.

Corresponding author address: Prof. Lynn M. Russell, Scripps Institution of Oceanography, University of California, San Diego, 9500 Gilman Dr., La Jolla, CA 92093-0221.
E-mail: lmrussell@ucsd.edu

Aerosols affect climate directly through scattering and absorbing solar radiation and indirectly by altering cloud microphysical properties (Haywood and Boucher 2000; Lohmann and Feichter 2005; Myhre et al. 2013). Natural aerosols are particularly important because they account for 70% of the global aerosol loading (Satheesh and Moorthy 2005) and result in uncertainty in aerosol–cloud–precipitation interactions (Carslaw et al. 2013; Yang et al. 2016a). Understanding the interactions between natural aerosols and climate is essential for

accurately assessing the impacts of anthropogenic aerosols on clouds and climate in present and future conditions.

Sea salt is one of the most important natural aerosols, which has the strongest production rate (Blanchard and Woodcock 1980), constitutes the largest fraction of natural aerosols by mass in the atmosphere (O'Dowd et al. 1997), and makes the largest contribution to the aerosol optical depth (AOD) in clean remote regions (Haywood et al. 1999; Mulcahy et al. 2008). It can also be an important source of cloud condensation nuclei (CCN) in remote marine areas (Clarke et al. 2006).

Sea salt aerosol exerts large radiative effects both on global and regional scales. Rap et al. (2013) used an aerosol microphysics model together with a radiative transfer model to estimate radiative effects of natural aerosols. They found sea salt exhibits a large aerosol direct effect, with a global averaged value of -0.44 W m^{-2} at the top of atmosphere, followed by -0.23 W m^{-2} for dimethyl sulfide (DMS)-derived sulfate and -0.21 W m^{-2} for volcanic sulfate. Korhonen et al. (2010) used a global aerosol microphysics model driven by reanalysis data to report that increases in sea salt emissions due to decadal increases in Southern Hemisphere wind speeds caused a summertime radiative forcing of -0.7 W m^{-2} between 50° and 65°S since the 1980s, which is similar in magnitude but opposite in sign to that from increases in CO_2 over the same period.

Sea salt emissions depend on both wind speed and sea surface temperature (O'Dowd and Smith 1993; Mårtensson et al. 2003; Geever et al. 2005; Clarke et al. 2006). Penner et al. (2001) found that a warmer climate may induce increases in sea salt emissions globally from 3340 Tg in 2000 to 5880 Tg in 2100 through increasing wind speed. Jones et al. (2007) reported that, in response to a doubling of CO_2 in a coupled climate model, increases in sea salt concentrations were found at high latitudes owing to stronger winds caused by the reduction in sea ice. Climate variability, such as El Niño–Southern Oscillation (ENSO), can also influence sea salt emissions and therefore sea salt concentrations. On interannual time scales, ENSO is the strongest signal of the ocean–atmosphere system (Wang et al. 1999). ENSO consists of periodic departures from expected sea surface temperature (SST) distributions in the equatorial Pacific Ocean. Although it is mainly a tropical event, ENSO dominates interannual variability globally and affects the weather and climate conditions in many remote regions through influencing pressure systems, winds, and precipitation. Assessing climate change requires knowledge of the full range of natural variability in ENSO phenomenon (Cobb et al. 2003). Xu et al. (2015) found that, through the Community Earth System Model (CESM) simulation, changes in sea salt

concentrations between positive and negative ENSO events were mainly driven by sea salt emissions. From the Law Dome ice core in East Antarctica, Vance et al. (2013) reported a statistically significant correlation between ENSO and sea salt during summer resulting from the reduced zonal wind speed over the South Pacific and the circumpolar high latitudes in El Niño conditions.

A number of recent studies have found that variations in natural aerosol emissions could influence ENSO variability. However, most of them focused on the stratospheric aerosols, such as volcanic aerosols. Using proxy data, Adams et al. (2003) and McGregor et al. (2010) found tropical volcanic eruptions, which inject SO_2 directly into the stratosphere, largely increased the probability of El Niño and reduced the zonal SST gradient along the equatorial Pacific by reducing surface insolation. Through model simulations, many studies also found that tropical volcanic emissions enhanced El Niño (Mann et al. 2005; Ohba et al. 2013; Maher et al. 2015; Stevenson et al. 2016) or La Niña (McGregor and Timmermann 2011; Zanchettin et al. 2012) events. The effects of tropospheric and stratospheric aerosols are expected to differ dramatically, and there has been very little work on the tropospheric aerosol–ENSO connection. By including an interactive aerosol scheme in the CSIRO climate model, Rotstayn et al. (2010) found the CSIRO model captured ENSO-induced rainfall variability in Australia better than in other models; they suggested that improvement is due to the role of interactive dust. In Rotstayn et al. (2011), they showed that the accurate simulation of the ENSO–rainfall relationship resulted from the anomalies in radiative forcing by dust, which decreased (increased) surface evaporation and caused less (more) rainfall in El Niño (La Niña) years over Australia.

Variations in sea salt emissions strongly influence sea salt concentrations and the corresponding aerosol radiative effects, which may also influence ENSO variability. However, few previous studies have considered the role of variations in sea salt emissions. In this study, correlation and spectrum analysis of a set of two 150-yr preindustrial simulations by the CESM are used to examine ENSO-induced changes in sea salt emissions between El Niño and La Niña events and the impacts of interannual variations in sea salt emissions on ENSO variability. We quantify 1) ENSO-induced interannual variations in sea salt emissions over the 150 years of simulation, 2) effects of interannual variations in sea salt emissions on ENSO variability, and 3) changes in circulation and precipitation rate due to ENSO-induced interannual variations in sea salt emissions. In this work, we focus on sea salt emissions and El Niño/La Niña

events in preindustrial conditions (for the year 1850 emissions) to avoid the influences of anthropogenic emissions. The interannual variations in this study are over 150 years of simulation, which are mainly driven by El Niño and La Niña signals. In this study, the main focus is on the Pacific regions because the El Niño (La Niña) cycle mainly occurs over the tropical Pacific and is sometimes referred to as Pacific warm (cold) episodes.

CESM and numerical experiments are described in section 2. Section 3 provides an analysis of ENSO-induced interannual variations in sea salt emissions. Section 4 investigates influences of interannual variations in sea salt emissions on ENSO variability by comparing simulations with and without interactive sea salt emissions. Section 5 presents the changes in circulation and precipitation between El Niño and La Niña events due to interannual variations in sea salt emissions. Section 6 summarizes these results.

2. Model description and experimental design

Simulations were performed using CESM, version 1.2.1, which includes components from Earth's atmosphere, ocean, land, land ice, and sea ice (Hurrell et al. 2013). The atmospheric model used here is the Community Atmosphere Model, version 5 (CAM5), with resolution of 1.9° latitude by 2.5° longitude and 30 vertical layers ranging from the surface to 3.6 hPa. The ocean component used here is a three-dimensional active model (Smith et al. 2010). The CESM-CAM5 treats the properties and processes of major aerosol components (sea salt, mineral dust, sulfate, black carbon, primary organic matter, and secondary organic aerosol) in the modal aerosol module (MAM3; Liu et al. 2012). Aerosol size distributions are represented by three lognormal modes: Aitken ($0.015\text{--}0.053\,\mu\text{m}$), accumulation ($0.058\text{--}0.27\,\mu\text{m}$), and coarse ($0.80\text{--}3.65\,\mu\text{m}$) modes. Mass mixing ratios of different aerosol species and the number mixing ratio are predicted for each mode. Aerosol optical properties are parameterized according to Ghan and Zaveri (2007). Activation of cloud droplets occurs on a multimodal lognormal aerosol size distribution based on the scheme of Abdul-Razzak and Ghan (2000). The model physically treats aerosol–cloud interactions using two-moment stratiform cloud microphysics, which predicts number concentrations and mixing ratios of cloud water and ice (Morrison and Gettelman 2008; Gettelman et al. 2010). The influence of aerosols on cloud microphysics has been quantified by Wang et al. (2012) and Ghan et al. (2016). The emissions of sea salt particles with diameter $<2.8\,\mu\text{m}$ are parameterized in terms of 10-m wind speed and sea surface temperature (Mårtensson et al. 2003). For diameters $>2.8\,\mu\text{m}$,

the emissions depend only on 10-m wind speed (Monahan et al. 1986). A more detailed description of the model aerosol representation can be found in Liu et al. (2012). In the simulations of this study, the radiation subroutine is calculated both with and without aerosol scattering and absorption. The aerosol radiative effects could be calculated from the differences of these two sets of radiation outputs. Only the radiation subroutine with aerosol scattering and absorption is used for the climate calculation.

To quantify the effects of interannual variations in sea salt emissions on ENSO variability, the following 150-yr simulations are performed:

- 1) IRUN: the standard simulation of preindustrial conditions using interactive (I) emissions. Emissions of sea salt are driven by the meteorological fields, which vary year to year.
- 2) ERUN: the sensitivity simulation of preindustrial conditions using prescribed emissions (E) of sea salt. The sea salt emissions in this simulation are interpolated in time between the 12 monthly mean values derived from the 150-yr IRUN simulation and do not change with the actual yearly values of wind or temperature. Hence, this simulation contains no interannual variability of sea salt emissions. The model setup is otherwise the same as that in IRUN.

To characterize the intensity of an El Niño/La Niña event, the Niño-3.4 index is used in this study, which is calculated as the averaged SST anomaly over the Niño-3.4 region ($5^\circ\text{S}\text{--}5^\circ\text{N}$, $170^\circ\text{--}120^\circ\text{W}$). An El Niño (La Niña) event in this study is characterized by a 3-month running mean of the monthly Niño-3.4 index that is above (below) the threshold of $+0.4^\circ\text{C}$ (-0.4°C) (Trenberth 1997). The standard deviations of the monthly Niño-3.4 index are 1.14 and 1.03 in IRUN and ERUN, respectively. In the 150-yr IRUN and ERUN simulations, 506 (720) and 514 (639) of the 1800 months are identified as El Niño (La Niña) events, respectively. This difference between IRUN and ERUN results from the feedback of removing interannual variations of sea salt emissions in ERUN. It is interesting that the number of months with total El Niño/La Niña (El Niño plus La Niña) events in IRUN is larger than that of ERUN, indicating that interannual variations in sea salt emissions may induce larger variations in Niño-3.4 index and enhance ENSO variability.

3. ENSO-induced interannual variations in sea salt emissions

Empirical orthogonal function (EOF) analysis of yearly anomalies of the simulated sea salt emissions

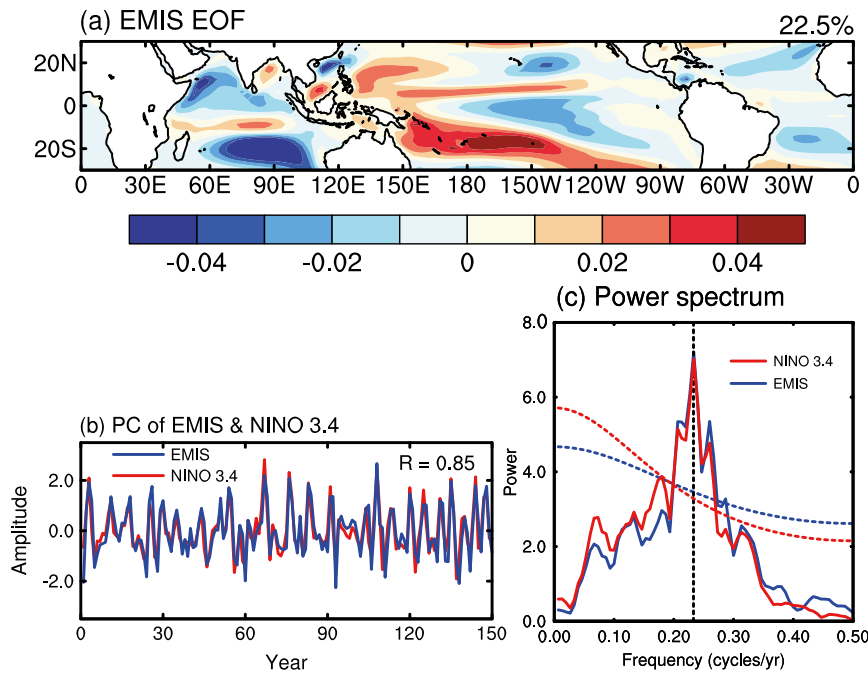


FIG. 1. (a) The leading EOF mode of simulated yearly sea salt emissions (EMIS) in the IRUN simulation. The variance explained by the leading-mode EOF is given at the top-right corner of the panel. (b) The time series of the PC of the leading-mode EOF of simulated yearly sea salt emissions (blue line) and the Niño-3.4 index (red line) in the IRUN simulation. The correlation coefficient between the Niño-3.4 index and PC of EOF of sea salt emissions is shown in the top-right corner of the panel. (c) The power spectrum of PC of EOF of simulated sea salt emissions and power spectrum of the Niño-3.4 index. The corresponding dashed lines indicate the 95% significance levels.

between 30°S and 30°N from the IRUN simulation is used to examine the influence of ENSO on sea salt emissions (Fig. 1). The leading EOF explains 22.5% of the interannual variations in the simulated sea salt emissions. Over the equatorial central-eastern Pacific Ocean, the EOF shows a negative pattern, while positive patterns of EOF are located over two bands off the equator around 20°S and 10°N and the tropical western Pacific Ocean, suggesting that opposing variations in sea salt emissions occurred in these two regions. This spatial pattern is similar to the SST anomaly during ENSO events, indicating that ENSO may influence sea salt emissions over the tropical Pacific Ocean. Figure 1b presents time series of the principal component (PC) of the leading EOF of sea salt emissions and the Niño-3.4 index calculated based on the simulated SST in the IRUN simulation. The leading PC is strongly correlated with the Niño-3.4 index, with the statistically significant correlation coefficient of +0.85, implying that ENSO strongly affects the interannual variations in sea salt emissions over the tropical Pacific in the CESM model. Figure 1c shows the power spectrum of the Niño-3.4 index and leading PC of yearly anomalies of sea salt

emissions. Both sea salt emissions and the Niño-3.4 index have a period of 4.3 years per cycle (0.23 cycles per year), suggesting that ENSO dominates interannual variations in sea salt emissions between 30°S and 30°N.

Figure 2 presents the composite differences in 10-m wind speed from ERA-Interim at the European Centre for Medium-Range Weather Forecasts (ECMWF) and the IRUN simulation between El Niño and La Niña events, which explains the mechanism of ENSO-induced interannual variations in sea salt emissions. Unless otherwise specified, the composite difference in this article refers to the difference between El Niño and La Niña events. The 10-m wind speed has been found to have large influences on rain-aerosol relationships through changing sea salt emissions (Yang et al. 2016a). The model captures well the pattern of differences in observed 10-m wind speed between 60°S and 60°N. During El Niño events, 10-m wind speed decreases over the equatorial central-eastern Pacific Ocean, in agreement with the feature of weakened easterly trade winds around the equator during the warm phase of ENSO (Wang et al. 2012). Wind speed increases over two bands off the equator around 20°S and 10°N and over the

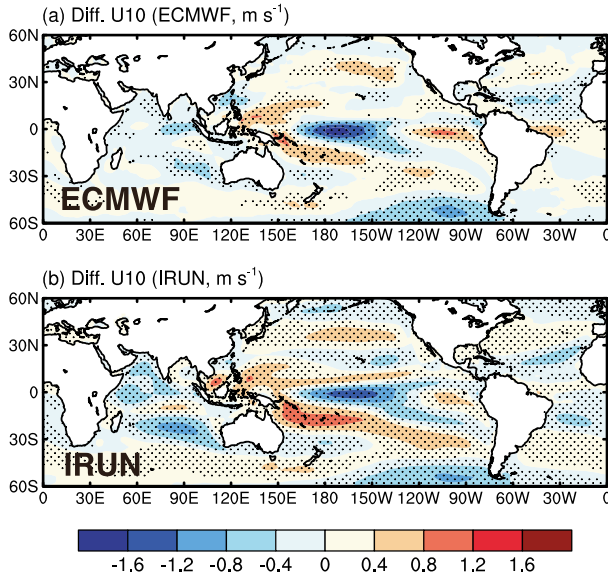


FIG. 2. Composite differences between El Niño and La Niña events for 10-m wind speed (U_{10} ; $m s^{-1}$) from (a) ERA-Interim and (b) the IRUN simulation. ECMWF reanalysis data used here are from 1979 to 2014. Significance levels are determined according to the Wilcoxon rank-sum test, and values that are significant at 95% are stippled.

tropical western Pacific Ocean relative to those during La Niña events, leading to the changes in sea salt emissions over these regions. Although changes in SST also affect sea salt emissions with diameter $<2.8\mu m$ in

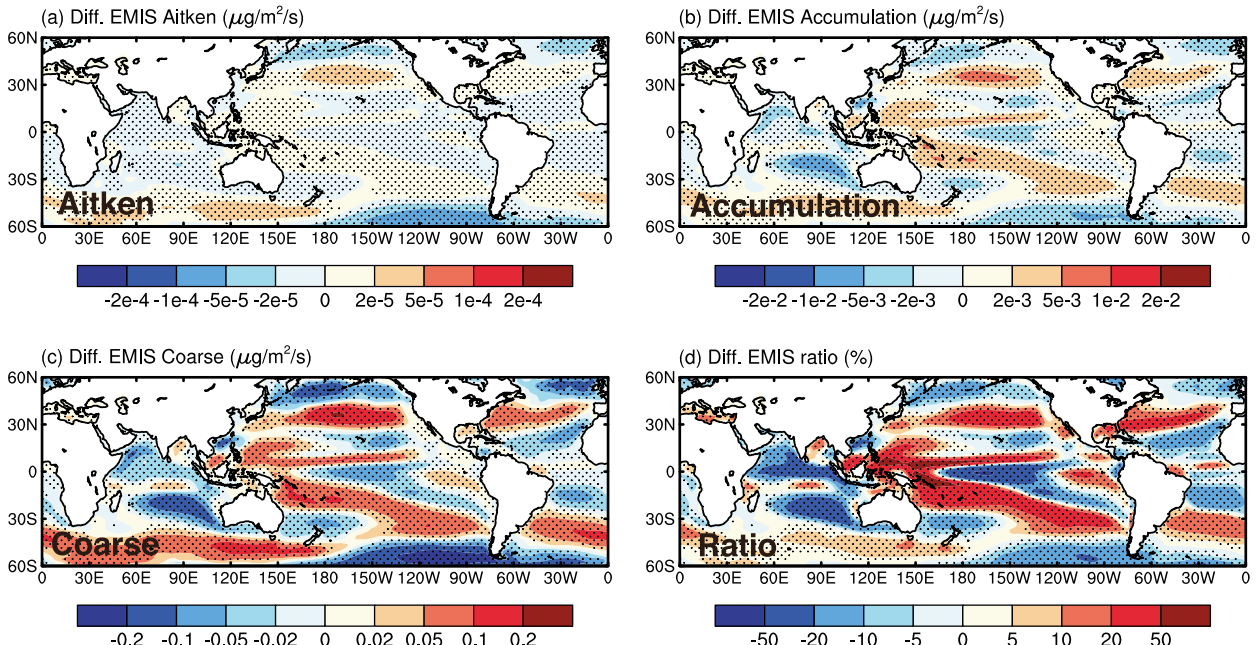


FIG. 3. Composite differences between El Niño and La Niña events in sea salt emissions in (a) Aitken, (b) accumulation, and (c) coarse modes ($\mu g m^{-2} s^{-1}$), and (d) the ratio of the differences in sea salt emissions relative to the 150-yr-averaged values in the IRUN simulation. Significance levels are determined according to the Wilcoxon rank-sum test, and values that are significant at 95% are stippled.

the model, its impact is smaller than that of wind speed (Mårtensson et al. 2003; Xu et al. 2015).

Figures 3a–c show the composite differences between El Niño and La Niña events in sea salt emissions in Aitken, accumulation, and coarse modes, respectively. The differences in sea salt emissions in three different modes show a similar spatial pattern but different magnitudes. The coarse mode shows the largest differences, followed by the accumulation and Aitken modes. Figure 3d presents the percentage differences in sea salt emissions relative to the 150-yr-averaged values in the IRUN simulation. The emissions in El Niño events are lower than those in La Niña events by 20%–50% over the tropical central-eastern Pacific Ocean and higher by 20%–50% over two bands off the equator around 20°S and 10°N and the tropical western Pacific Ocean. Over the equatorial Pacific, ENSO-induced differences in sea salt emissions between El Niño and La Niña events are even larger than 50%. These changes in sea salt emissions can also have feedback effects on ENSO variability.

4. Influences of interannual variations in sea salt emissions on ENSO variability

Before investigating the influences of interannual variations in sea salt emissions on ENSO variability, it is important to evaluate the model ability to simulate the interannual variations in sea salt emissions. Because of

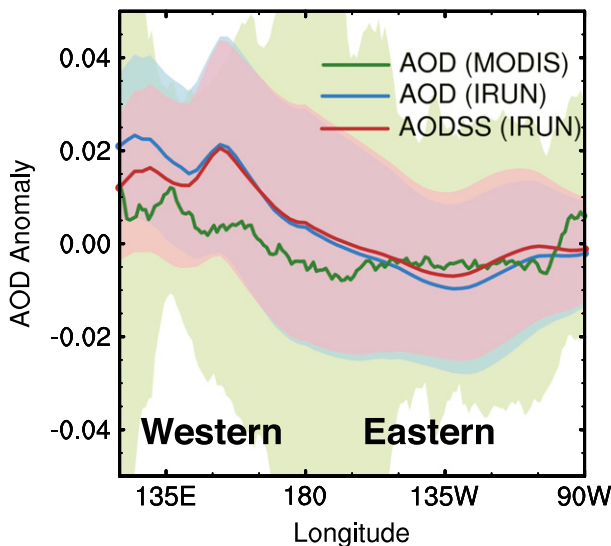


FIG. 4. Composite differences between El Niño and La Niña events in AOD averaged between 20°S and 20°N derived from MODIS (green line) data and the IRUN simulation (blue line) and in AOD of sea salt from the IRUN simulation (red line). Temporal mean values are shown in lines with $\pm\sigma$ (standard deviation) shown in light color areas. MODIS AOD data used here are from 2001 to 2014.

the lack of sea salt emission measurements, AOD data are used here to represent sea salt emissions indirectly. Figure 4 shows the AOD composite differences between El Niño and La Niña events averaged between 20°S and 20°N derived from the Moderate Resolution Imaging Spectroradiometer (MODIS) satellite and the IRUN simulation. The model reproduces the observed pattern of lower AOD over the tropical eastern Pacific Ocean and higher AOD over the tropical western Pacific Ocean during El Niño events compared to those during La Niña events. However, the differences are higher by a factor of 2 in the model than in the satellite-observed AOD. This discrepancy probably results from the uncertainties in both model and satellite data, including emission parameterizations and aerosol–cloud–precipitation interactions in the model, and signal uncertainty, retrieval bias, and cloud contamination in satellite data. The MODIS data used here cover only 14 yr, which only contain four El Niño events (2002/03, 2004/05, 2006/07, and 2009/10) and three La Niña events (2007/08, 2010/11, and 2011/12). The comparisons of the model simulations and satellite observations are therefore limited by the higher sampling error of the satellite dataset. The model overprediction of ENSO signal and SST anomaly (Otto-Bliesner et al. 2016) also contributes to the larger AOD variability and may cause some biases to our results. Differences in AOD from sea salt aerosol are almost the same as those from all aerosols

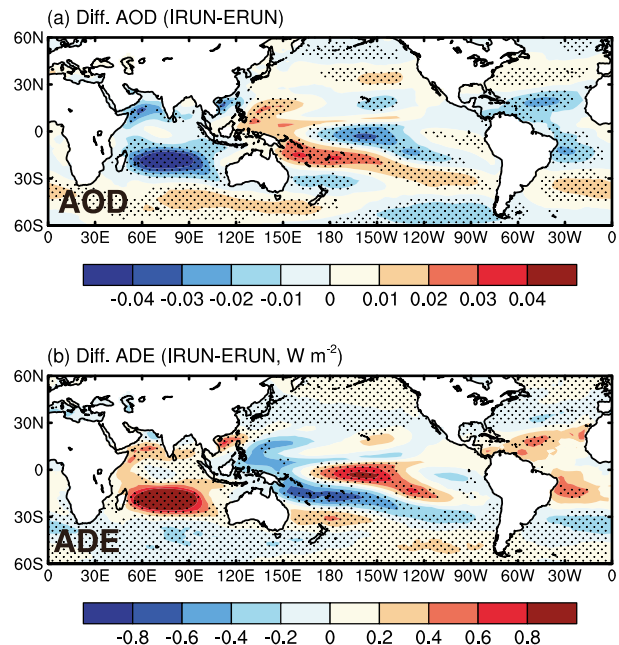


FIG. 5. Changes due to differences in sea salt emissions between El Niño and La Niña events in simulated (a) AOD and (b) aerosol direct radiative effects (ADE) at the top of atmosphere (W m^{-2}). Significance levels are determined according to the Wilcoxon rank-sum test, and values that are significant at 95% are stippled.

combined, indicating that sea salt has the largest contributions to the variations in AOD over the tropical Pacific Ocean in preindustrial conditions in the model. Note that MODIS AOD should also be influenced by impact of ENSO on biomass burning over the Maritime Continent. The simulation does not include that influence because the simulation is for preindustrial conditions and lacks interannual variability in biomass burning emissions.

Figure 5 shows the changes in simulated AOD and aerosol direct radiative effects (ADE) at the top of the atmosphere due to the differences in sea salt emissions between El Niño and La Niña events. Aerosol direct radiative effects are calculated as changes in shortwave radiative flux with and without scattering and absorption by aerosols (Ghan 2013). The spatial pattern of the changes in AOD is similar to that of differences in sea salt emissions (Fig. 3d), with the maximum decrease of more than -0.03 over the equatorial central-eastern Pacific Ocean and $+0.03$ increase over the tropical western Pacific during El Niño events compared to those during La Niña events. These changes in AOD lead to increases in radiative fluxes into the atmosphere of more than $+0.8 \text{ W m}^{-2}$ over the equatorial central-eastern Pacific Ocean and decreases in radiative fluxes in the range from -0.4 to -0.8 W m^{-2} over the tropical

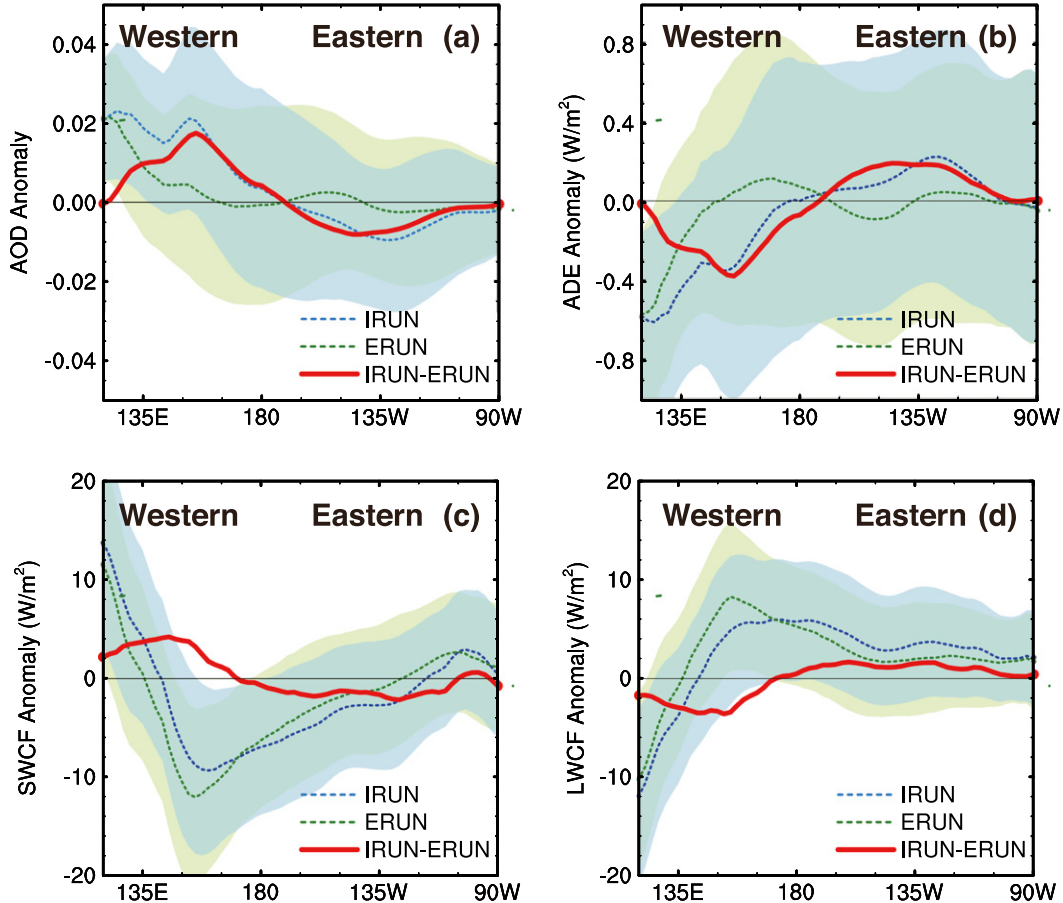


FIG. 6. Composite differences between El Niño and La Niña events averaged between 20°S and 20°N for the IRUN (blue lines) and ERUN (green lines) simulations as well as the changes in these differences due to the interannual variations in sea salt emissions (red lines) in (a) simulated AOD, (b) ADE, (c) CRE_{SW} , and (d) CRE_{LW} . Temporal mean values are shown in lines with $\pm\sigma$ (standard deviation) shown in light color areas.

western Pacific during El Niño events compared to those during La Niña events. These changes in radiative fluxes result from the interannual variations in sea salt emissions.

Figure 6 presents composite differences between El Niño and La Niña events in AOD, ADE, and shortwave and longwave cloud radiative effects (CRE_{SW} and CRE_{LW}) averaged between 20°S and 20°N in the IRUN and ERUN simulations, as well as the changes in these differences due to interannual variations in sea salt emissions. The cloud radiative effect is defined as the difference of net downward radiative flux between all sky and clear sky at the top of the atmosphere. Relative to La Niña events, AOD during El Niño events is lower by 0.01 over 130°W and higher by about 0.02 over 155°E between 20°S and 20°N in the IRUN simulation. In the ERUN simulation, the differences in AOD between El Niño and La Niña events are less than 0.005 between

150°E and 90°W over the tropics. The larger AOD response to changes in ENSO phase in the IRUN simulation is due to the interannual variations in sea salt emissions. These changes in AOD between IRUN and ERUN further increase radiative fluxes into the atmosphere by $+0.2 \text{ W m}^{-2}$ over the tropical eastern Pacific and decrease radiative fluxes with the maximum value of -0.4 W m^{-2} over the tropical western Pacific, owing to interannual variations in sea salt emissions. Cloud radiative effects exert large variations between El Niño and La Niña events. During El Niño events, CRE_{SW} (CRE_{LW}) presents anomalous cooling (heating) over most of the tropical Pacific Ocean and anomalous heating (cooling) over the Maritime Continent compared to La Niña events. Variations in sea salt emissions also perturb the cooling and heating of cloud radiative effects through changing SST and cloud fraction, and their roles are larger than aerosol–cloud interactions

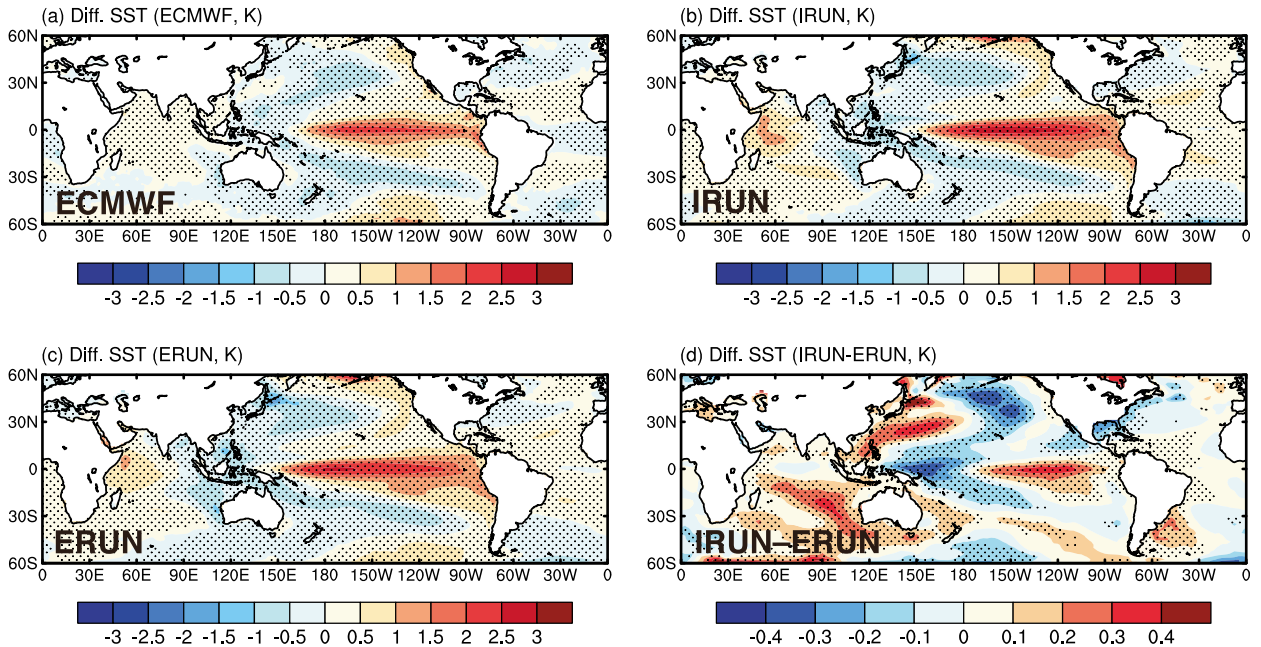


FIG. 7. Composite differences between El Niño and La Niña events in SST (K) from (a) ERA-Interim, the (b) IRUN and (c) ERUN simulations, and (d) the changes in SST due to the interannual variations in sea salt emissions. ECMWF reanalysis data used here are from 1979 to 2014. Significance levels are determined according to the Wilcoxon rank-sum test, and values that are significant at 95% are stippled.

over the tropics. A more detailed analysis of impacts of natural aerosols on cloud radiative effect variability can be found in Yang et al. (2016b).

Figure 7 shows composite differences between El Niño and La Niña events in SST from ERA-Interim and the IRUN and ERUN simulations, as well as the changes in SST due to interannual variations in sea salt emissions. The model captures the SST pattern of anomalously warm SST across the tropical eastern Pacific during El Niño events. However, the model overestimates the SST over the tropical eastern Pacific during El Niño events, as also reported by Otto-Btiesner et al. (2016). This overestimation of SST anomalies could also result in the overestimation of the ENSO-sea salt feedback in CESM. The interannual variations in sea salt emissions lead to increases (decreases) in SST by 0.2–0.4 K over the tropical eastern (western) Pacific Ocean, enhancing the differences in SST between El Niño and La Niña events. This contribution to SST anomalies suggests that interannual variations in sea salt emissions enhance ENSO variability.

Spectral analysis of the Niño-3.4 index in the IRUN and ERUN simulations was performed in order to evaluate the extent to which sea salt emissions could influence the ENSO variability (Fig. 8). ENSO shows the same period of 4.3 years per cycle for both the IRUN and ERUN simulations, indicating that interannual variation in sea salt emissions do not change the period

of the ENSO cycle. However, the ENSO in the IRUN simulation shows more power than that in the ERUN simulation. In addition, the standard deviation of the monthly Niño-3.4 index is 1.14 in IRUN, larger than that

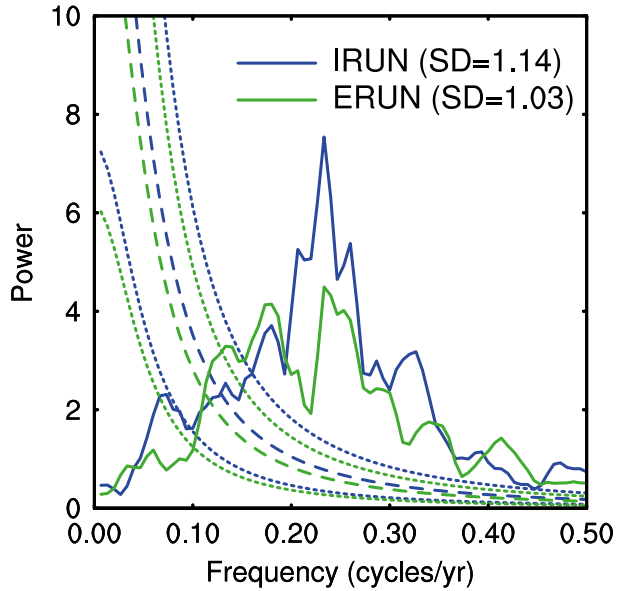


FIG. 8. Power spectrum of the Niño-3.4 index in the IRUN and ERUN simulations. The corresponding dashed and dotted lines indicate the “red noise” curve, with upper and lower confidence bounds at the 95% and 5% significance levels, respectively. Standard deviations of the Niño-3.4 index are shown in the top-right corner.

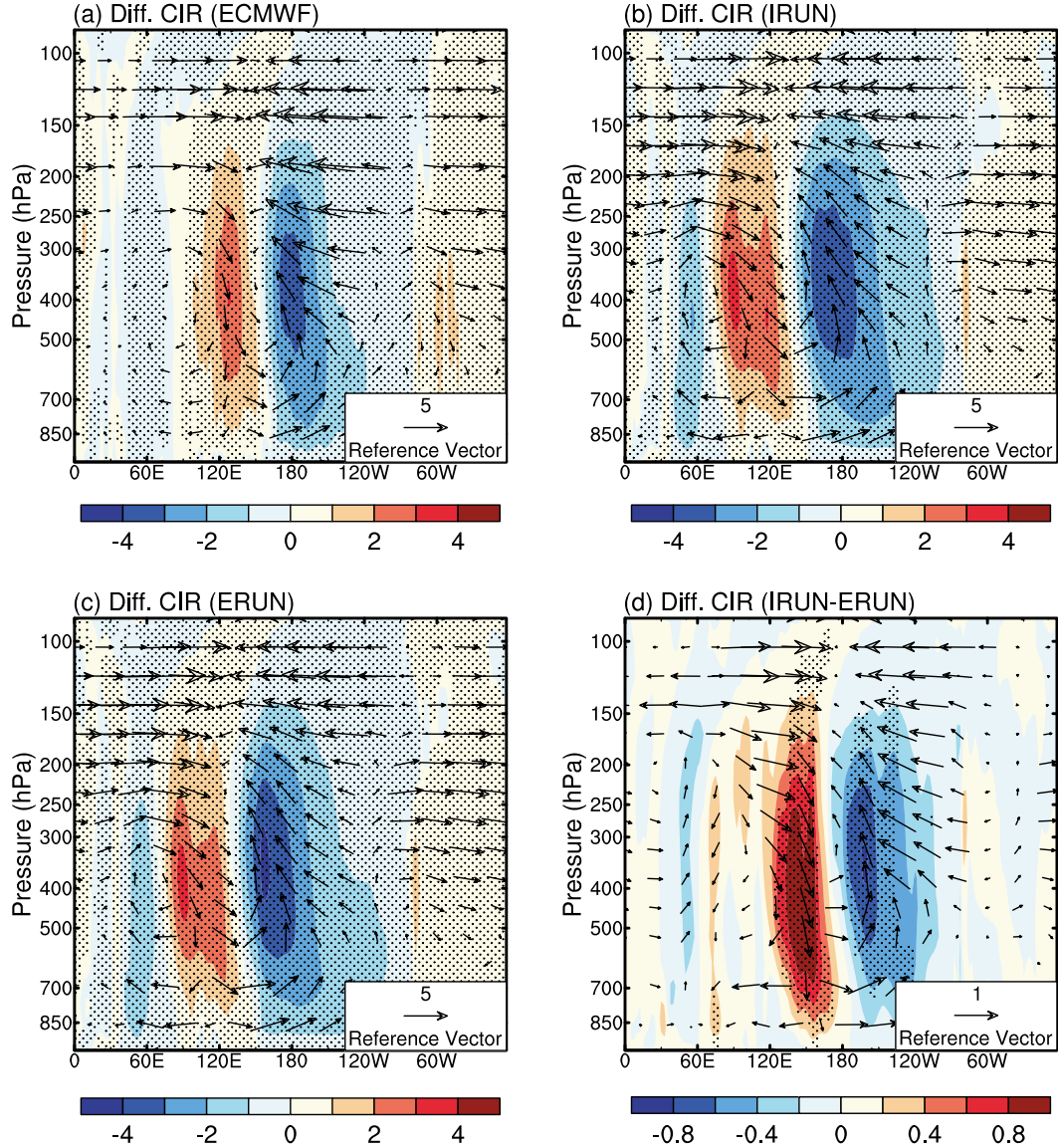


FIG. 9. Composite differences between El Niño and La Niña events in vertical velocity (contours; Pa s^{-1}) scaled by a factor of 100 averaged between 10°S and 10°N from (a) ERA-Interim, the (b) IRUN and (c) ERUN simulations, and (d) the changes in vertical velocity due to the interannual variations in sea salt emissions. Overlying vectors represent the zonal wind (m s^{-1}) and the vertical velocity (Pa s^{-1}) scaled by a factor of -100 . ECMWF reanalysis data used here are from 1979 to 2014. Significance levels are determined according to the Wilcoxon rank-sum test, and values that are significant at 95% are stippled.

of 1.03 in ERUN by 10%. During El Niño events, the Niño-3.4 index increases from 1.18 to 1.36 when including interannual variations in sea salt emissions, and these differences are statistically significant at the 95% confidence level. These differences provide additional support for the result that interannual variations in sea salt emissions enhance ENSO variability by 10%. The weakened (strengthened) wind speed during the enhanced El Niño events causes more decreases (increases) in sea salt emissions over the tropical eastern (western)

Pacific. This effect further enhances ENSO variability, resulting in a positive sea salt emission–ENSO feedback.

5. Interannual variations in sea salt emissions affect circulation and precipitation

The atmospheric Walker circulation is a conceptual model of the airflow in the tropics, which is related to the east–west SST gradient along the equator. Figure 9 presents the differences in Walker circulation between

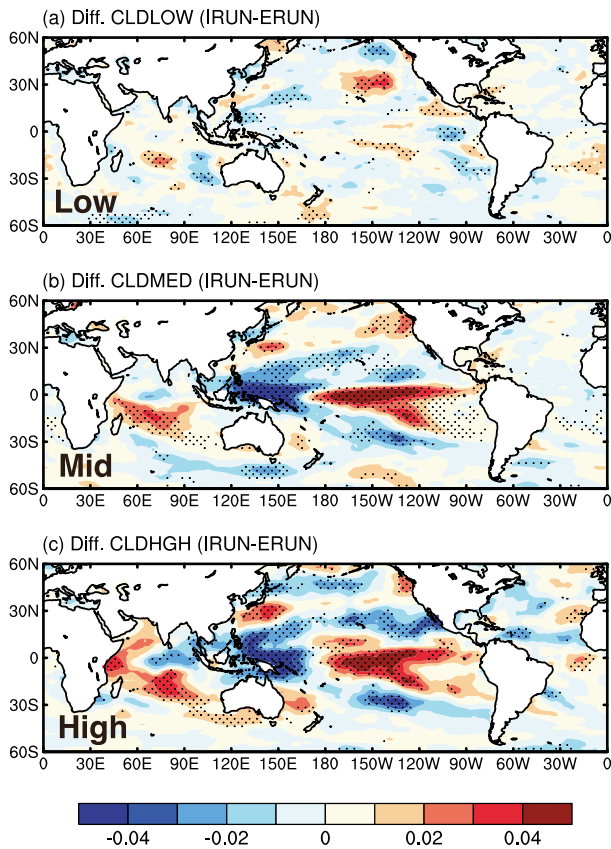


FIG. 10. Changes in simulated (a) low, (b) midlevel, and (c) high cloud fraction due to the changes in sea salt emissions between El Niño and La Niña events.

El Niño and La Niña events in ERA-Interim and the IRUN and ERUN simulations, as well as the changes in the Walker circulation due to the interannual variations in sea salt emissions. During El Niño events, the model reproduced the observed strong ascent over the equatorial central Pacific Ocean (Figs. 9a–c). Interannual variations in sea salt emissions produce anomalous ascent over the equatorial eastern Pacific and subsidence over the equatorial western Pacific between El Niño and La Niña events (Fig. 9d), corresponding to changes in SST (Fig. 7d). These changes in vertical motions weaken both the downward motions over the eastern Pacific Ocean and the strong upward motions over the Maritime Continent of the Walker circulation.

The effects of interannual variations in sea salt emissions on ascent and subsidence between El Niño and La Niña events result in different cloud fractions and precipitation rates. Figure 10 shows changes in simulated cloud fractions due to the changes in sea salt emissions between El Niño and La Niña events. During El Niño events, the large cloud fraction over the tropics is

associated with the stronger and deeper convection, driven by warmer SST. Interannual variations in sea salt emissions lead to changes in vertical motion and induce large differences in mid- and high-level cloud fractions. The mid- and high-level cloud fractions increase over the tropical eastern Pacific Ocean and decrease over the tropical western Pacific Ocean, with maximum differences larger than 0.04. For low-level cloud, the cloud fraction shows smaller differences. These changes in cloud fraction caused by interannual variations in sea salt emissions enhance the interannual variations in cloud fractions and, consequently, enhance the interannual variations in cloud radiative effects, which were also reported by Yang et al. (2016b).

Figure 11 presents composite differences between El Niño and La Niña events of simulated convective and stratiform precipitation rate and the associated changes in precipitation rate due to interannual variations in sea salt emissions. The model captures the typical features of the higher convective precipitation rate by $2\text{--}6 \text{ mm day}^{-1}$ over the tropical Pacific Ocean and lower by $2\text{--}4 \text{ mm day}^{-1}$ over the Maritime Continent during El Niño events relative to those during La Niña events (Figs. 11a,c). With interannual variations in sea salt emissions in the IRUN simulation, the convective precipitation was enhanced by $0.6\text{--}1.2 \text{ mm day}^{-1}$ over the tropical central-eastern Pacific Ocean and weakened by $0.9\text{--}1.5 \text{ mm day}^{-1}$ over the Maritime Continent (Fig. 11e), partly enhancing the differences in precipitation between El Niño and La Niña events. The spatial pattern of changes in convective precipitation caused by interannual variations in sea salt emissions is almost the same as those of mid- and high-level cloud fractions (Figs. 10b,c), suggesting that impacts of interannual variations in sea salt emissions on precipitation rate are mainly through changing cloud fraction. For stratiform clouds, the differences in precipitation rate between El Niño and La Niña events (Figs. 11b,d) and the differences caused by interannual variations in sea salt emissions (Fig. 11f) have spatial patterns similar to those of convective precipitation but are lower by one order of magnitude. This further indicates that sea salt emission effects on precipitation over the tropics are not a result of the aerosol–cloud–precipitation microphysical interactions but instead are the result of the feedback effects of the radiative changes. One caution in interpreting these results is that the model only treats aerosol effects on stratiform clouds, which may limit the scope of their interactions with cloud and precipitation. The increases (decreases) in precipitation over the tropical central-eastern Pacific Ocean (the Maritime Continent) (Figs. 11e,f) that result from interannual variations in sea salt emissions will

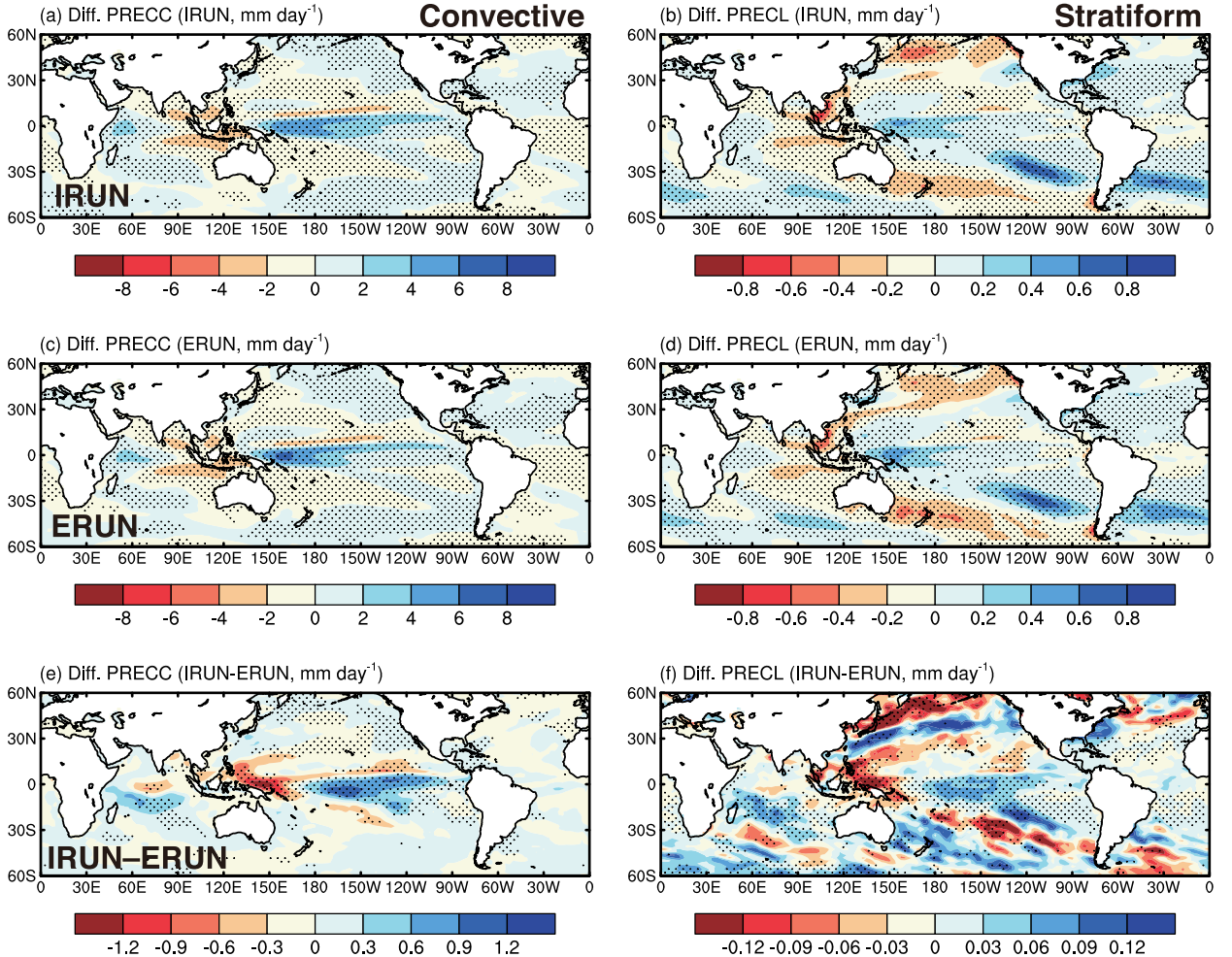


FIG. 11. Composite differences between El Niño and La Niña events in simulated (left) convective and (right) stratiform precipitation rates from the (a),(b) IRUN and (c),(d) ERUN simulations, as well as (e),(f) the changes in precipitation rate due to interannual variations in sea salt emissions. Significance levels are determined according to the Wilcoxon rank-sum test, and values that are significant at 95% are stippled.

further lead to increased (decreased) wet deposition of sea salt particles and decreased (increased) sea salt concentrations over these regions, reinforcing the positive sea salt emission–ENSO feedback.

6. Conclusions

This study examines the interactions between interannual variations in sea salt emissions and El Niño–Southern Oscillation (ENSO) using 150-yr simulations in preindustrial conditions from the CESM model. EOF patterns of sea salt emissions are similar to the SST anomalies during ENSO events, indicating that El Niño/La Niña events may influence sea salt emissions over the tropical Pacific Ocean in the simulation with interactive sea salt emissions. The PC of the leading EOF of sea salt emissions is strongly correlated with the Niño-3.4 index,

with the statistically significant correlation coefficient of +0.85. In addition, both sea salt emissions and the Niño-3.4 index have a period of 4.3 years per cycle, suggesting that ENSO has a strong impact on the interannual variations in sea salt emissions between 30°S and 30°N. ENSO-induced changes in 10-m wind speed decrease the sea salt emissions by 20%–50% over the tropical central-eastern Pacific Ocean and increase the emissions by 20%–50% over two bands off the equator around 20°S and 10°N and the tropical western Pacific Ocean during El Niño events compared to those in La Niña events. The coarse mode shows larger differences in emissions between El Niño and La Niña events than the Aitken and accumulation modes.

The model successfully reproduces the pattern from MODIS satellite observations of lower AOD over the tropical eastern Pacific Ocean and higher AOD over the

tropical western Pacific Ocean during El Niño events compared to La Niña events. Interannual variations in sea salt emissions lead to decreases (increases) in AOD by 0.03 over the equatorial central-eastern (western) Pacific Ocean during El Niño events compared to La Niña events. These changes in AOD further lead to increases in radiative fluxes into the atmosphere by $+0.2 \text{ W m}^{-2}$ over the tropical eastern Pacific and decreases in radiative fluxes with a maximum value of -0.4 W m^{-2} over the tropical western Pacific. SST increases (decreases) by 0.2–0.4 K over the tropical eastern (western) Pacific Ocean enhancing the differences in SST between El Niño and La Niña events. From power spectrum analysis, ENSO has more power in the simulation with interactive sea salt emissions compared to the simulation without interactive sea salt emissions. The standard deviation of the Niño-3.4 index increased by 10% when considering interannual variations in sea salt emissions, indicating that interannual variations in sea salt emissions enhance ENSO variability by 10%.

The interannual variations in sea salt emissions result in changes in SST that also produce ascent over the equatorial eastern Pacific and subsidence over the equatorial western Pacific during El Niño events. These changes in vertical motions weaken the Walker circulation. The mid- and high-level cloud fractions increase over the tropical eastern Pacific Ocean and decrease over the tropical western Pacific Ocean because of the interannual variations in sea salt emissions. With interannual variations in sea salt emissions, the convective precipitation is enhanced by $0.6\text{--}1.2 \text{ mm day}^{-1}$ over the tropical central-eastern Pacific Ocean and weakened by $0.9\text{--}1.5 \text{ mm day}^{-1}$ over the Maritime Continent, partly enhancing the differences in precipitation between El Niño and La Niña events.

Many previous studies have examined the influence of ENSO on aerosols, but few of them focused on the effects of aerosols on ENSO. In this study, the interactions between sea salt emissions and ENSO have been discussed in the loop illustrated in Fig. 12. First, in the tropical central-eastern Pacific, El Niño is associated with lower wind speeds than La Niña. This leads to decreased sea salt emissions, decreased aerosol optical depth, and a positive anomaly in aerosol direct radiative effect. This translates into increases in SST (a more powerful ENSO), decreased wind speeds, increased vertical velocities, increased mid/high cloud cover, and increased precipitation. The decreased wind speeds and increased precipitation further result in decreased sea salt emissions and concentrations, reinforcing the ENSO signal. This loop introduces a positive sea salt emission–ENSO feedback,

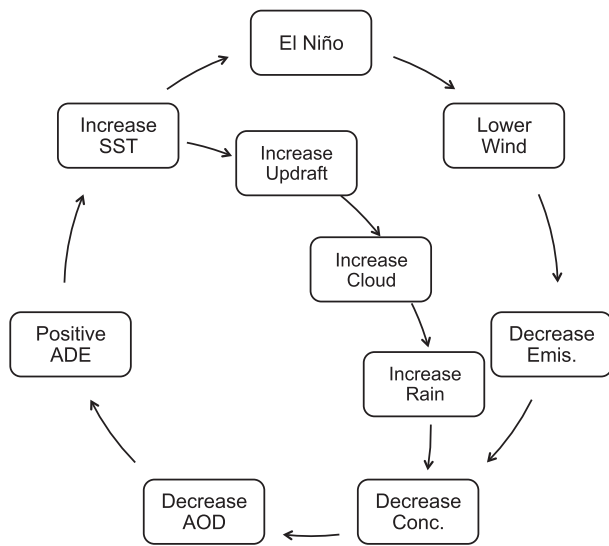


FIG. 12. Positive sea salt emission–ENSO feedback.

which is an important addition to the understanding of ENSO.

This study examined the impacts of interannual variations in sea salt emissions on ENSO variability. The results presented here are from the CESM model, which does not include aerosol effects on convective clouds in the present version. This may limit the extent of aerosol microphysical impacts on precipitation. A more comprehensive sea salt emission–ENSO interaction could be completed if future models include aerosol effects on convective clouds. In addition to changing radiative fluxes and SST, the interannual variations in sea salt emissions may also perturb ocean dynamic processes. It is worth noting that anthropogenic climate change is associated with changes in ENSO characteristics (Collins et al. 2010; Cai et al. 2015). Strong centennial modulations also exist in unforced ENSO simulations (Wittenberg 2009; Stevenson et al. 2010, 2012). Stevenson et al. (2012) found the ENSO variability weakened with increasing CO₂, but the changes are insignificant owing to both external forcing and natural variability. The changes of ENSO power between IRUN and ERUN at the frequency of 0.23 cycles per year is slightly larger than the power range of ENSO for 1850 ensemble simulations of Community Climate System Model, version 4 (CCSM4), in Stevenson et al. (2012), which supports the results in this study. However, the results presented in this study may be caused by both sea salt emission–ENSO feedback and centennial modulations of ENSO; a larger ensemble and longer time simulations are needed to isolate these effects. The results are obtained using the CESM model and should be confirmed using other climate models. The results in this

study are from 150-yr simulations in preindustrial conditions, which differ from modern conditions. In addition to the tropical Pacific, this study shows the potential impacts of natural aerosols on climate variability over the Indian Ocean (Figs. 7d and 11e), which should be examined in future studies.

Acknowledgments. This research was supported by National Science Foundation AGS1048995 and by DOE DE-SC0006679 as part of the U.S. Department of Energy, Office of Science, Biological and Environmental Research, Decadal and Regional Climate Prediction using Earth System Models (EaSM) program. The Pacific Northwest National Laboratory is operated for the DOE by Battelle Memorial Institute under Contract DE-AC05-76RLO 1830. The National Energy Research Scientific Computing Center (NERSC) provided computational resources. We acknowledge support from the DOE, Office of Science, Biological and Environmental Research, as part of the Regional and Global Climate Modeling program. The reanalysis data are obtained from ERA-Interim at the European Centre for Medium-Range Weather Forecasts (ECMWF; accessed 6 October 2016; <http://apps.ecmwf.int/datasets/>). The data and codes for these results are posted at the NERSC repository (accessed 6 October 2016; http://portal.nersc.gov/project/m1374/Seasalt_ENSO).

REFERENCES

- Abdul-Razzak, H., and S. J. Ghan, 2000: A parameterization of aerosol activation: 2. Multiple aerosol types. *J. Geophys. Res.*, **105**, 6837–6844, doi:[10.1029/1999JD901161](https://doi.org/10.1029/1999JD901161).
- Adams, J. B., M. E. Mann, and C. M. Ammann, 2003: Proxy evidence for an El Niño-like response to volcanic forcing. *Nature*, **426**, 274–278, doi:[10.1038/nature02101](https://doi.org/10.1038/nature02101).
- Blanchard, D. C., and A. H. Woodcock, 1980: The production, concentration and vertical distribution of the sea-salt aerosols. *Ann. N. Y. Acad. Sci.*, **338**, 330–347, doi:[10.1111/j.1749-6632.1980.tb17130.x](https://doi.org/10.1111/j.1749-6632.1980.tb17130.x).
- Cai, W., and Coauthors, 2015: ENSO and greenhouse warming. *Nat. Climate Change*, **5**, 849–859, doi:[10.1038/nclimate2743](https://doi.org/10.1038/nclimate2743).
- Carslaw, K. S., and Coauthors, 2013: Large contribution of natural aerosols to uncertainty in indirect forcing. *Nature*, **503**, 67–71, doi:[10.1038/nature12674](https://doi.org/10.1038/nature12674).
- Clarke, A. D., S. R. Owens, and J. Zhou, 2006: An ultrafine sea-salt flux from breaking waves: Implications for cloud condensation nuclei in the remote marine atmosphere. *J. Geophys. Res.*, **111**, D06202, doi:[10.1029/2005JD006565](https://doi.org/10.1029/2005JD006565).
- Cobb, K. M., C. D. Charles, H. Cheng, and R. L. Edwards, 2003: El Niño–Southern Oscillation and tropical Pacific climate during the last millennium. *Nature*, **424**, 271–276, doi:[10.1038/nature01779](https://doi.org/10.1038/nature01779).
- Collins, M., and Coauthors, 2010: The impact of global warming on the tropical Pacific and El Niño. *Nat. Geosci.*, **3**, 391–397, doi:[10.1038/ngeo868](https://doi.org/10.1038/ngeo868).
- Geever, M., C. D. O'Dowd, S. van Ekeren, R. Flanagan, D. E. Nilsson, G. de Leeuw, and Ü. Rannik, 2005: Submicron sea spray fluxes. *Geophys. Res. Lett.*, **32**, L15810, doi:[10.1029/2005GL023081](https://doi.org/10.1029/2005GL023081).
- Gettelman, A., and Coauthors, 2010: Global simulations of ice nucleation and ice supersaturation with an improved cloud scheme in the Community Atmosphere Model. *J. Geophys. Res.*, **115**, D18216, doi:[10.1029/2009JD013797](https://doi.org/10.1029/2009JD013797).
- Ghan, S. J., 2013: Technical note: Estimating aerosol effects on cloud radiative forcing. *Atmos. Chem. Phys.*, **13**, 9971–9974, doi:[10.5194/acp-13-9971-2013](https://doi.org/10.5194/acp-13-9971-2013).
- , and R. A. Zaveri, 2007: Parameterization of optical properties for hydrated internally mixed aerosol. *J. Geophys. Res.*, **112**, D10201, doi:[10.1029/2006JD007927](https://doi.org/10.1029/2006JD007927).
- , and Coauthors, 2016: Challenges in constraining anthropogenic aerosol effects on cloud radiative forcing using present-day spatiotemporal variability. *Proc. Natl. Acad. Sci. USA*, **113**, 5804–5811, doi:[10.1073/pnas.1514036113](https://doi.org/10.1073/pnas.1514036113).
- Haywood, J., and O. Boucher, 2000: Estimates of the direct and indirect radiative forcing due to tropospheric aerosols: A review. *Rev. Geophys.*, **38**, 513–543, doi:[10.1029/1999RG000078](https://doi.org/10.1029/1999RG000078).
- , V. Ramaswamy, and B. J. Soden, 1999: Tropospheric aerosol climate forcing in clear-sky satellite observations over the oceans. *Science*, **283**, 1299–1303, doi:[10.1126/science.283.5406.1299](https://doi.org/10.1126/science.283.5406.1299).
- Hurrell, J. W., and Coauthors, 2013: The Community Earth System Model: A framework for collaborative research. *Bull. Amer. Meteor. Soc.*, **94**, 1339–1360, doi:[10.1175/BAMS-D-12-00121.1](https://doi.org/10.1175/BAMS-D-12-00121.1).
- Jones, A., J. M. Haywood, and O. Boucher, 2007: Aerosol forcing, climate response and climate sensitivity in the Hadley Centre climate model. *J. Geophys. Res.*, **112**, D20211, doi:[10.1029/2007JD008688](https://doi.org/10.1029/2007JD008688).
- Korhonen, H., K. S. Carslaw, P. M. Forster, S. Mikkonen, N. D. Gordon, and H. Kokkola, 2010: Aerosol climate feedback due to decadal increases in Southern Hemisphere wind speeds. *Geophys. Res. Lett.*, **37**, L02805, doi:[10.1029/2009GL041320](https://doi.org/10.1029/2009GL041320).
- Liu, X., and Coauthors, 2012: Toward a minimal representation of aerosols in climate models: Description and evaluation in the Community Atmosphere Model CAM5. *Geosci. Model Dev.*, **5**, 709–739, doi:[10.5194/gmd-5-709-2012](https://doi.org/10.5194/gmd-5-709-2012).
- Lohmann, U., and J. Feichter, 2005: Global indirect aerosol effects: A review. *Atmos. Chem. Phys.*, **5**, 715–737, doi:[10.5194/acp-5-715-2005](https://doi.org/10.5194/acp-5-715-2005).
- Maher, N., S. McGregor, M. H. England, and A. S. Gupta, 2015: Effects of volcanism on tropical variability. *Geophys. Res. Lett.*, **42**, 6024–6033, doi:[10.1002/2015GL064751](https://doi.org/10.1002/2015GL064751).
- Mann, M. E., M. A. Cane, S. E. Zebiak, and A. Clement, 2005: Volcanic and solar forcing of the tropical Pacific over the past 1000 years. *J. Climate*, **18**, 447–456, doi:[10.1175/JCLI-3276.1](https://doi.org/10.1175/JCLI-3276.1).
- Mårtensson, E. M., E. D. Nilsson, G. de Leeuw, L. H. Cohen, and H.-C. Hansson, 2003: Laboratory simulations and parameterization of the primary marine aerosol production. *J. Geophys. Res.*, **108**, 4297, doi:[10.1029/2002JD002263](https://doi.org/10.1029/2002JD002263).
- McGregor, S., and A. Timmermann, 2011: The effect of explosive tropical volcanism on ENSO. *J. Climate*, **24**, 2178–2191, doi:[10.1175/2010JCLI3990.1](https://doi.org/10.1175/2010JCLI3990.1).
- , —, and O. Timm, 2010: A unified proxy for ENSO and PDO variability since 1650. *Climate Past*, **6**, 1–17, doi:[10.5194/cp-6-1-2010](https://doi.org/10.5194/cp-6-1-2010).
- Monahan, E. C., D. E. Spiel, and K. L. Davidson, 1986: A model of marine aerosol generation via whitecaps and wave disruption. *Oceanic Whitecaps*, E. Monahan and G. M. Niocaill, Eds., D. Reidel, 167–174.
- Morrison, H., and A. Gettelman, 2008: A new two-moment bulk stratiform cloud microphysics scheme in the Community

- Atmosphere Model, version 3 (CAM3). Part I: Description and numerical tests. *J. Climate*, **21**, 3642–3659, doi:[10.1175/2008JCLI2105.1](https://doi.org/10.1175/2008JCLI2105.1).
- Mulcahy, J. P., C. D. O'Dowd, S. G. Jennings, and D. Ceburnis, 2008: Significant enhancement of aerosol optical depth in marine air under high wind conditions. *Geophys. Res. Lett.*, **35**, L16810, doi:[10.1029/2008GL034303](https://doi.org/10.1029/2008GL034303).
- Myhre, G. D., and Coauthors, 2013: Anthropogenic and natural radiative forcing. *Climate Change 2013: The Physical Science Basis*, T. F. Stocker et al., Eds., 659–740.
- O'Dowd, C., and M. H. Smith, 1993: Physicochemical properties of aerosols over the northeast Atlantic: Evidence for wind-speed-related submicron sea-salt aerosol production. *J. Geophys. Res.*, **98**, 1137–1149, doi:[10.1029/92JD02302](https://doi.org/10.1029/92JD02302).
- , —, I. E. Consterdine, and J. A. Lowe, 1997: Marine aerosol, sea salt, and the marine sulphur cycle: A short review. *Atmos. Environ.*, **31**, 73–80, doi:[10.1016/S1352-2310\(96\)00106-9](https://doi.org/10.1016/S1352-2310(96)00106-9).
- Ohba, M., H. Shiogama, T. Yokohata, and M. Watanabe, 2013: Impact of strong tropical volcanic eruptions on ENSO simulated in a coupled GCM. *J. Climate*, **26**, 5169–5182, doi:[10.1175/JCLI-D-12-00471.1](https://doi.org/10.1175/JCLI-D-12-00471.1).
- Otto-Btiesner, B. L., and Coauthors, 2016: Climate variability and change since 850 CE: An ensemble approach with the Community Earth System Model. *Bull. Amer. Meteor. Soc.*, **97**, 735–754, doi:[10.1175/BAMS-D-14-00233.1](https://doi.org/10.1175/BAMS-D-14-00233.1).
- Penner, J. E., and Coauthors, 2001: Aerosols, their direct and indirect effects. *Climate Change 2001: The Scientific Basis*, J. T. Houghton et al., Eds., Cambridge University Press, 289–348.
- Rap, A., C. E. Scott, D. V. Spracklen, N. Bellouin, P. M. Forster, K. S. Carslaw, A. Schmidt, and G. Mann, 2013: Natural aerosol direct and indirect radiative effects. *Geophys. Res. Lett.*, **40**, 3297–3301, doi:[10.1002/grl.50441](https://doi.org/10.1002/grl.50441).
- Rotstayn, L. D., M. A. Collier, M. R. Dix, Y. Feng, H. B. Gordon, S. P. O'Farrell, I. N. Smith, and J. Syktus, 2010: Improved simulation of Australian climate and ENSO-related rainfall variability in a global climate model with an interactive aerosol treatment. *Int. J. Climatol.*, **30**, 1067–1088, doi:[10.1002/joc.1952](https://doi.org/10.1002/joc.1952).
- , —, R. M. Mitchell, Y. Qin, S. K. Campbell, and S. M. Dravitzki, 2011: Simulated enhancement of ENSO-related rainfall variability due to Australian dust. *Atmos. Chem. Phys.*, **11**, 6575–6592, doi:[10.5194/acp-11-6575-2011](https://doi.org/10.5194/acp-11-6575-2011).
- Satheesh, S. K., and K. K. Moorthy, 2005: Radiative effects of natural aerosols: A review. *Atmos. Environ.*, **39**, 2089–2110, doi:[10.1016/j.atmosenv.2004.12.029](https://doi.org/10.1016/j.atmosenv.2004.12.029).
- Smith, R., and Coauthors, 2010: The Parallel Ocean Program (POP) reference manual. Los Alamos National Laboratory Tech. Rep. LAUR-10-01853, 141 pp. [Available online at <http://www.cesm.ucar.edu/models/cesm1.0/pop2/doc/sci/POPRefManual.pdf>.]
- Stevenson, S., B. Fox-Kemper, M. Jochum, B. Rajagopalan, and S. Yeager, 2010: Model ENSO validation using wavelet probability analysis. *J. Climate*, **23**, 5540–5547, doi:[10.1175/2010JCLI3609.1](https://doi.org/10.1175/2010JCLI3609.1).
- , —, R. Neale, C. Deser, and G. Meehl, 2012: Will there be a significant change to El Niño in the twenty-first century? *J. Climate*, **25**, 2129–2145, doi:[10.1175/JCLI-D-11-00252.1](https://doi.org/10.1175/JCLI-D-11-00252.1).
- , B. Otto-Btiesner, J. Fasullo, and E. Brady, 2016: “El Niño like” hydroclimate responses to last millennium volcanic eruptions. *J. Climate*, **29**, 2907–2921, doi:[10.1175/JCLI-D-15-0239.1](https://doi.org/10.1175/JCLI-D-15-0239.1).
- Trenberth, K. E., 1997: The definition of El Niño. *Bull. Amer. Meteor. Soc.*, **78**, 2771–2777, doi:[10.1175/1520-0477\(1997\)078<2771:TDOENO>2.0.CO;2](https://doi.org/10.1175/1520-0477(1997)078<2771:TDOENO>2.0.CO;2).
- Vance, T. R., T. D. van Ommen, M. A. J. Curran, C. T. Plummer, and A. D. Moy, 2013: A millennial proxy record of ENSO and eastern Australian rainfall from the Law Dome ice core, East Antarctica. *J. Climate*, **26**, 710–725, doi:[10.1175/JCLI-D-12-00003.1](https://doi.org/10.1175/JCLI-D-12-00003.1).
- Wang, C., C. Deser, J.-Y. Yu, P. DiNezio, and A. Clement, 2012: El Niño–Southern Oscillation (ENSO): A review. *Coral Reefs of the Eastern Pacific*, P. Glynn, D. Manzello, and I. Enochs, Eds., Springer Science, 3–19.
- Wang, H., R. Zhang, J. Cole, and F. Chavez, 1999: El Niño and the related phenomenon Southern Oscillation (ENSO): The largest signal in interannual climate variation. *Proc. Natl. Acad. Sci. USA*, **96**, 11 071–11 072, doi:[10.1073/pnas.96.20.11071](https://doi.org/10.1073/pnas.96.20.11071).
- Wittenberg, A. T., 2009: Are historical records sufficient to constrain ENSO simulations? *Geophys. Res. Lett.*, **36**, L12702, doi:[10.1029/2009GL038710](https://doi.org/10.1029/2009GL038710).
- Xu, L., and Coauthors, 2015: Interannual to decadal climate variability of sea salt aerosols in the coupled climate model CESM1.0. *J. Geophys. Res. Atmos.*, **120**, 1502–1519, doi:[10.1002/2014JD022888](https://doi.org/10.1002/2014JD022888).
- Yang, Y., L. M. Russell, S. Lou, Y. Liu, B. Singh, and S. J. Ghan, 2016a: Rain–aerosol relationships influenced by wind speed. *Geophys. Res. Lett.*, **43**, 2267–2274, doi:[10.1002/2016GL067770](https://doi.org/10.1002/2016GL067770).
- , and Coauthors, 2016b: Impacts of ENSO events on cloud radiative effects in preindustrial conditions: Changes in cloud fraction and their dependence on interactive aerosol emissions and concentrations. *J. Geophys. Res. Atmos.*, **121**, 6321–6335, doi:[10.1002/2015JD024503](https://doi.org/10.1002/2015JD024503).
- Zanchettin, D., C. Timmreck, H.-F. Graf, A. Rubino, S. Lorenz, K. Lohmann, K. Krüger, and J. H. Jungclaus, 2012: Bi-decadal variability excited in the coupled ocean–atmosphere system by strong tropical volcanic eruptions. *Climate Dyn.*, **39**, 419–444, doi:[10.1007/s00382-011-1167-1](https://doi.org/10.1007/s00382-011-1167-1).